JOURNAL OF GEOPHYSICAL RESEARCH, VOL. 114, D06304, doi:10.1029/2008JD010270, 2009

Detection of a tropospheric ozone anomaly using a newly developed ozone retrieval algorithm for an up-looking infrared interferometer

K. J. Lightner,[1,2] W. W. McMillan,[1] K. J. McCann,[1] R. M. Hoff,[1] M. J. Newchurch,[3] E. J. Hintsa,[4] and C. D. Barnet[5]

Received 14 April 2008; revised 12 December 2008; accepted 29 December 2008; published 25 March 2009.

[1] On 2 June 2003, the Baltimore Bomem Atmospheric Emitted Radiance Interferometer (BBAERI) recorded an infrared spectral time series indicating the presence of a tropospheric ozone anomaly. The measurements were collected during an Atmospheric Infrared Sounder (AIRS) validation campaign called the 2003 AIRS BBAERI Ocean Validation Experiment (ABOVE03) conducted at the United States Coast Guard Chesapeake Light station located 14 miles due east of Virginia Beach, Virginia (36.91°N, 75.71°W). Ozone retrievals were performed with the Kurt Lightner Ozone BBAERI Retrieval (KLOBBER) algorithm, which retrieves tropospheric column ozone, surface to 300 mbar, from zenith-viewing atmospheric thermal emission spectra. KLOBBER is modeled after the AIRS retrieval algorithm consisting of a synthetic statistical regression followed by a physical retrieval. The physical retrieval is implemented using the k-Compressed Atmospheric Radiative Transfer Algorithm (kCARTA) to compute spectra. The time series of retrieved integrated ozone column on 2 June 2003 displays spikes of about 10 Dobson units, well above the error of the KLOBBER algorithm. Using instrumentation at Chesapeake Light, satellite imaging, trace gas retrievals from satellites, and Potential Vorticity (PV) computations, it was determined that these sudden increases in column ozone likely were caused by a combination of midtropospheric biomass burning products from forest fires in Siberia, Russia, and stratospheric intrusion by a tropopause fold occurring over central Canada and the midwestern United States.

Citation: Lightner, K. J., W. W. McMillan, K. J. McCann, R. M. Hoff, M. J. Newchurch, E. J. Hintsa, and C. D. Barnet (2009), Detection of a tropospheric ozone anomaly using a newly developed ozone retrieval algorithm for an up-looking infrared interferometer, *J. Geophys. Res.*, *114*, D06304, doi:10.1029/2008JD010270.

1. Introduction

[2] The troposphere in the Northern Hemisphere midlatitudes contains an average ozone mixing ratio of 40 to 80 parts per billion by volume (ppbv) at the surface [*Lefohn et al.*, 2001], while the midlatitude tropopause ozone mixing ratio ranges from 90 ppbv to 400 ppbv [*Newchurch et al.*, 2003]. Because of the photochemical nature of tropospheric ozone, the above-mentioned values can vary greatly as a result of atmospheric pollution. Stratospheric intrusion can also have a significant effect on the ozone content of the upper troposphere [*Newchurch et al.*, 2003]. The largest production rate of tropospheric ozone in the Northern Hemisphere results from photochemical oxidation of pollution [*Parrish et al.*, 1993; *Marenco*, 1986]. A significant body of literature exists illustrating the negative effects on human health from prolonged exposure to ozone [*McConnell et al.*, 2002; *Kehrl et al.*, 1999; *McDonnell et al.*, 1991; *Gong et al.*, 1986]. This fact makes the ability to monitor ozone from an up-looking ground-based thermal instrument capable of running 24 h a day, desirable.

[3] Ozone in the troposphere comes from 2 main sources: (1) photochemical production from atmospheric pollution and (2) transport from the stratosphere to the troposphere. Folding can occur between the stratosphere and troposphere as a result of strong frontal systems and associated convective storms penetrating the tropopause. It is estimated as much as 6×10^{11} kg of ozone per year is circulated down from the stratosphere, globally [*Sudo and Takahashi*, 2001; *Olsen and Stanford*, 2001]. A third source of tropospheric ozone comes from photochemical reactions of naturally occurring NO_x produced by microbial activity in the soil and from lightning [*Sinha and Toumi*, 1997].

[4] The reactions producing tropospheric ozone differ from those in the stratosphere through the lack of UV

[1]Department of Physics, University of Maryland Baltimore County, Baltimore, Maryland, USA.
[2]Now at Applied Signal Technology, Inc., Annapolis Junction, Maryland, USA.
[3]Department of Atmospheric Science, University of Alabama in Huntsville, Huntsville, Alabama, USA.
[4]Woods Hole Oceanographic Institution, Woods Hole, Massachusetts, USA.
[5]STAR, NESDIS, NOAA, Camp Springs, Maryland, USA.

0148-0227/09/2008JD010270$09.00

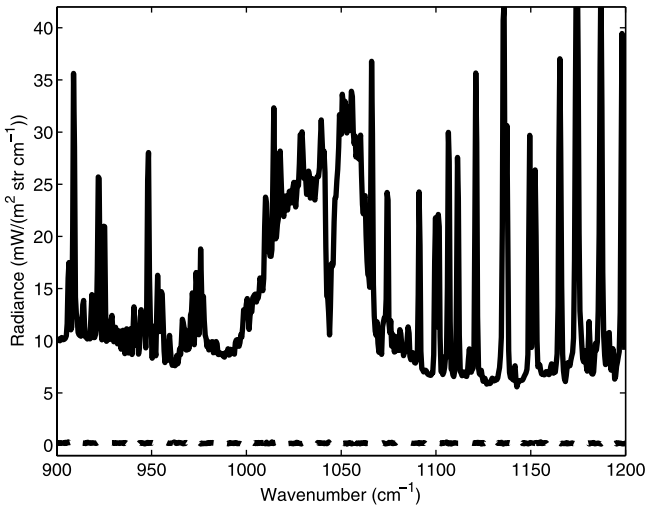

Figure 1. BBAERI spectrum measured on 2 June at 1400 UTC at Chesapeake Light. The solid black line shows the portion of the spectrum used by KLOBBER to retrieve ozone. The dashed line shows the average noise radiance of 0.18 mW/(m^2 sr cm^{-1}).

radiation required to dissociate tropospheric O_2. Instead, atomic oxygen needed for tropospheric ozone production forms by dissociation of nitrogen dioxide, NO_2. When hit with photons of $\lambda \leq 390$ nm, NO_2 dissociates [*Thompson*, 1984]. This wavelength of radiation exists in ample quantities in the troposphere because the overlying atmospheric layers do not efficiently absorb it. Once liberated, atomic oxygen can react with molecular oxygen to form ozone. This reaction accounts for almost all of the ozone produced in the troposphere [*Thompson*, 2003].

2. Instrument

[5] Building on the heritage of the University of Wisconsin-Madison built Atmospheric Emitted Radiance Interferometer (AERI) [*Feltz et al.*, 1998], BBAERI's infrared interferometer, front-end optics and calibration blackbodies were built by ABB Bomem of Quebec, Canada. In normal operation, the Bomem MR-100 interferometer has an Optical Path Difference (OPD) of 1.0371 cm resulting in a spectral point spacing of 0.4821 cm^{-1}. The detector assembly consists of a Stirling-cycle-cooled Mercury Cadmium Telluride (HgCdTe) and Indium Antimonide (InSb) sandwich. The HgCdTe detector provides spectral sensitivity from 525 cm^{-1} to 1800 cm^{-1} and the InSb provides sensitivity from 1800 cm^{-1} to 3000 cm^{-1}. Typical signal-to-noise ratios in the region of the spectrum used by KLOBBER range from 15 to 24 decibels (see Figure 1). During ABOVE03, infrared spectral measurements were made at zenith, 45° from zenith and 135° from zenith each having a field-of-view of about 10 degrees. The 135° and 45° views were used to measure sea surface temperature and emissivity [*Nalli et al.*, 2008]. Each cycle of the instrument included these three view angles as well as two calibration blackbody views. One calibration blackbody was held at a constant temperature of 60°C and the other was allowed to drift with the ambient temperature. Ambient temperature ranged from 15°C to 31°C with and average value of 23°C. The integration time for the zenith, 45° and 135° views was 2.5 min, 90 individual spectra. The blackbody views were each integrated for 1.25 min, 46 individual spectra. A zenith-viewing spectrum was acquired every 10 min.

3. Ozone Spectrum

[6] The O_3 molecule, like the H_2O molecule, is an asymmetric rotor giving rise to an extremely complex emission/absorption spectrum consisting of about 275,000 spectral lines within the 0 cm^{-1} to 4043 cm^{-1} region and approximately 30,000 lines in the 10 μm band alone [*Rothman et al.*, 1998]. Ozone exhibits three fundamental vibrational-rotational modes in the infrared spectrum ν_1, ν_2 and ν_3. These three modes manifest themselves as the symmetric stretch, the bending vibration and the antisymmetric stretch, respectively [*Herzberg*, 1971].

[7] The ν_1 band appears between 1100 cm^{-1} to 1200 cm^{-1} and ν_2 ranges from 630 cm^{-1} to 800 cm^{-1} [*Smith et al.*, 2001, 1997; *Devi et al.*, 1997]. Of these three bands the ν_3, located roughly between 1000 cm^{-1} and 1100 cm^{-1} displays the strongest emission/absorption and its P, Q and R branches give rise to the spectral feature of interest [*Smith et al.*, 2001; *De Backer-Barilly and Courtois*, 1997; *Flaud et al.*, 1987]. The KLOBBER algorithm uses measured spectra from 900 cm^{-1} through 1200 cm^{-1} to retrieve ozone (see Figure 1). Ozone lines in this region experience broadening proportional to pressure [*Engelen and Stephens*, 1997]. This fact, along with the large number of spectral lines and instrument spectral resolution, does not permit individual O_3 lines to be resolved by BBAERI, just the overall band shape.

4. Statistical Retrieval

[8] The KLOBBER regression uses synthetic "observations" to train the retrieval coefficients. The term synthetic means that the spectral "observations" are calculated. Eigenvector decomposition is utilized to constrain the final solution. The statistical retrieval and regression coefficient generation are discussed in the following paragraphs.

[9] The training set used in the retrieval consists of 2723 ozonesondes obtained from the Southern Hemispheric ADditional OZonesonde (SHADOZ) database and the Department of Atmospheric Science at the University of Alabama in Huntsville (see Table 1) [*Thompson et al.*, 2003a, 2003b; M. Newchurch, personal communication, 2003]. The synthetic spectral "observations" were calculated with the KCARTA forward model [*Strow et al.*, 1998]. The balloons were flown between 1994 to 2002 from 22 different sites around the world.

[10] The ozonesondes were conditioned before use in the spectral calculations. The temperature, water vapor and ozone profiles were all interpolated onto the AIRS 100 pressure levels [*Strow et al.*, 2003]. The AIRS pressure levels are used to establish a standard vertical axis. Since the balloons burst around 4 mbar, the full range of AIRS pressure levels is not attained. The Air Force Geophysical Laboratory (AFGL) 1976 U.S. standard atmosphere was used to fill in the missing data above the burst point of the balloons. Using a standard atmosphere above the burst point

Table 1. The 2723 Ozonesondes Used in the Statistical Retrieval Training Set

Location	Latitude	Longitude	Elevation (m)	Number of Cases
Ascension Island	7.98°S	14.42°W	91	169
Boulder, Colorado, USA	40.01°N	105.27°W	1743	371
Fairbanks, Alaska, USA	64.83°N	147.86°W	138	44
Hilo, Hawaii, USA	19.75°N	155.08°W	0	268
Houston, Texas, USA	29.98°N	95.33°W	181	52
Huntsville Al, USA	34.44°N	86.35°W	196	138
Irene, South Africa	25.90°S	28.22°E	1524	81
Kaashidhoo	4.97°N	73.47°E	1	54
La Réunion Island	21.06°S	55.48°E	24	79
Malindai, Kenya	2.99°S	40.19°E	−6	29
Nairobi, Kenya	1.27°S	36.80°WE	1795	90
Nashville, Tennessee, USA	36.13°N	86.77°W	180	41
Natal, Brazil	5.42°S	35.38°W	42	128
Pago Pago, American Samoa	14.23°S	170.56°W	77	145
Papeete, Tahiti	18.00°S	149.00°W	2	70
Paramaribo, Suriname	5.81°N	55.21°W	25	60
Sable Island, Canada	43.97°N	60.03°W	5	27
San Cristóbal	0.92°S	89.60°W	8	126
Suva, Fiji	18.13°S	178.40°E	6	145
Trinidad Head, California, USA	41.05°N	124.15°W	20	208
Wallops Island, Virginia, USA	37.83°N	75.49°W	2	361
Watukosek, Java	7.57°S	112.65°E	50	43

introduces a discontinuity in the profiles. The discontinuities are smoothed using a boxcar average across the vicinity of the burst point of the balloon. The lower portion of the profiles also were conditioned to fit the 100 levels. This conditioning took the surface values of temperature, water vapor and ozone to be the values at the AIRS pressure levels larger then the sonde ground pressure.

[11] Successful retrievals require the inputs to contain information about the quantity being retrieved. An earlier study shows ozone profile retrievals using ground-based infrared spectra to be difficult especially in the stratosphere [*Van Delst*, 1996]. Thus, accurate ozone retrievals need additional information about the ozone profile. The KLOBBER statistical retrieval uses the infrared spectrum from 900 cm^{-1} to 1200 cm^{-1}, the temperature profile, the water vapor profile, the stratospheric ozone profile from 100 mbar to the top of the atmosphere and a ground point ozone measurement. The statistical retrieval coefficients determine how much information, if any, is taken from each of the inputs. These five inputs form a single input column vector whose dimensions are 867 by 1,

$$r_i = [S(j) \quad T(k) \quad Os(m) \quad Og \quad Wv(n)]. \tag{1}$$

[12] In equation (1), the training set vector index, i, ranges from 1 to 2723, $S(j)$ represents the radiance input from 900 cm^{-1} to 1200 cm^{-1} where the spectral channel index, j, ranges from 1 to 622. $T(k)$ represents the temperature profile, degrees Kelvin, on the AIRS 100 pressure levels where the level index, k, ranges from 1 to 100. $Os(m)$ represents the natural logarithm of the stratospheric ozone mixing ratio profile, parts per million by volume, on the AIRS pressure levels from 100 mbar to the top of the atmosphere where the level index, m, ranges from 1 to 44. Og represents the natural logarithm of the surface ozone mixing ratio, parts per million by volume. $Wv(n)$ represents the water vapor mixing ratio profile, parts per million by volume, on the AIRS 100 pressure levels where the level index, n, ranges from 1 to 100.

[13] When generating the statistical retrieval coefficients, $S(j)$ was taken from the synthetic spectra and $T(k)$, $Os(m)$, Og and $Wv(n)$ were all taken from the training set ozonesondes. Using the logarithm of the ozone mixing ratio stabilizes the retrieval solutions by creating a more linear relationship between the input observations and the ozone mixing ratio at any one level in the profile [*Luo et al.*, 2002]. An additional advantage results by ensuring that the ozone mixing ratio solutions are always positive. Specifying stratospheric and surface ozone enables the retrieval to focus completely on tropospheric ozone, providing a huge advantage since spectral sensitivity tests using KCARTA show sensitivity in the 10 μm band of ozone resulting from both tropospheric and stratospheric ozone.

[14] The basic form of the retrieval consists of the simple matrix multiplication shown in equation (2). The matrix operator, A, describes the statistical relationship between the conditioned input observations, r, and the logarithm of the ozone mixing ratio, $ln(o)$, at each vertical point in the atmospheric profile. The raw input observations, r', are centered using the average synthetic "observation," $\bar{r}$, from the training set of 2723 synthetic spectra; see equations (3) and (4). The term "centered" refers to the process of subtracting the mean synthetic observation from the raw input observations.

$$\ln(o) = A \cdot U^T \cdot r, \tag{2}$$

$$r = r' - \bar{r}, \tag{3}$$

$$\bar{r} = \frac{1}{2723} \sum_{i=1}^{2723} r_i. \tag{4}$$

[15] The operator, U, is a unitary transformation matrix whose columns consist of the eigenvectors of the covariance of the 2723 synthetic " observations," r_i, from the training set. This unitary transformation matrix rotates the covariance matrix, C, resulting in a diagonal matrix, λ, with the eigenvalues of C as the diagonal entries; see equations (5) and (6). The symbol, $\otimes$, refers to the outer product.

$$C = \frac{1}{2723} \sum_{i=1}^{2723} (r_i - \bar{r}) \otimes (r_i - \bar{r})^T \tag{5}$$

$$U^T \cdot C \cdot U = \lambda. \tag{6}$$

Since the dimensions of each r_i is 867 by 1, the dimensions of U and C are 867 by 867. The term U^T refers to the transpose of U. By performing the retrieval in a rotated coordinate frame, the solutions produced by A can be constrained to smooth realistic solutions.

Table 2. Direct Versus Indirect Tropospheric Ozone Column Measured Using an Ozonesonde for Direct and the KLOBBER Retrieval Algorithm for Indirect[a]

Date in 2003	UTC Time	Ozonesonde (DU)	KLOBBER (DU)	Statistical % Error	Final % Error
2 June	21:56	46.1	45.6	−28.0	−1.1
3 June	7:00	42.3	45.4	−32.5	7.3
5 June	16:26	37.4	36.8	−24.2	−1.6
9 June	17:46	39.9	39.2	−33.4	−1.8
10 June	16:48	41.9	43.9	−10.7	4.8

[a]Column amounts, surface to 300 mbar, are expressed in Dobson units (DU). The last two columns show the percent error from the statistical retrieval and the final solution from the physical retrieval.

[16] Starting with equation (2), the coefficient matrix, A, can be generated using the ozone profiles from the training set, o_i, with synthetic input observations, r_i where the training set index, i, ranges from 1 to 2723. Equation (8) illustrates the method by which the 100 by 867 coefficient matrix, A, is generated.

$$A = \ln(o_i) \cdot r_i^T \cdot U \cdot \left(U^T \cdot C \cdot U + H\right)^{-1} \tag{7}$$

$$A = \ln(o_i) \cdot r_i^T \cdot U \cdot (\lambda + H)^{-1}. \tag{8}$$

[17] Substituting equation (6) into equation (7) results in equation (8). The diagonal matrix, H, in the above expressions allows the solutions produced by A to be controlled, or damped. The first 25 entries in H corresponding to the largest eigenvalues in λ, are set equal to zero. All other diagonal entries are given a value of 1×10^8. The factor of 1×10^8 was chosen arbitrarily. Applying large weights to eigenvectors with small eigenvalues effectively removes their contribution to the A operator. Because eigenvectors with small eigenvalues tend to introduce high-frequency oscillations into the solution, damping these eigenvectors constrains the solution.

[18] When performing the statistical retrieval on real data, the same process used to construct the multisensor input vectors described in equation (1) is used to construct the retrieval input vectors, r'_{BBAERI}. In r'_{BBAERI}, $S(j)$ consists of the measured BBAERI spectra. $T(k)$ and $Wv(n)$ consist of the retrieved BBAERI temperature and water vapor profiles interpolated onto the AIRS pressure levels. $Os(m)$ is derived from a climatology from the Stratospheric Aerosol and Gas Experiment II (SAGE II) interpolated on to the AIRS pressure levels (G. Labow, personal communication, 2002). Og is measured with ground-based ozone gas samplers. These gas samplers will be discussed later in this paper.

[19] The temperature and water vapor profiles are retrieved from each of the noncloudy, zenith-viewing BBAERI spectra, using the University of Wisconsin Madison's temperature and water vapor retrieval code first described in the literature in 1998 [*Feltz et al.*, 1998]. Since the temperature and water vapor profiles are not just retrieved using BBAERI spectra alone, the possibility of containing additional statistical information justifies their use. The SAGE II climatology was constructed by averaging profiles lying within ±2 degrees latitude and ±15 degrees longitude of the BBAERI site. The climatology is computed for each month of the year.

[20] The output ozone profile from the statistical retrieval, o_{stat}, is calculated by applying the retrieval coefficients, A, from equation (8) to a multisensor input vector, r'_{BBAERI}. Just as in equation (2), the multisensor input vector, r'_{BBAERI}, is centered using the average multisensor vector, $\bar{r}$, from the training set,

$$\ln(o_{stat}) = A \cdot U^T \cdot r_{BBAERI}, \tag{9}$$

$$r_{BBAERI} = r'_{BBAERI} - \bar{r}, \tag{10}$$

$$o_{stat} = e^{A \cdot U^T \cdot r_{BBAERI}}. \tag{11}$$

[21] The statistical retrieval alone does not produce satisfactory results for tropospheric column ozone; see Table 2. Thus, a physical retrieval algorithm was developed using the statistical retrieval as a first guess input for the tropospheric ozone profile. Because the KLOBBER algorithm is modeled after the AIRS science team algorithm, the process of using a physical retrieval to improve on the solution from a statistical retrieval was retained [*Susskind et al.*, 2003]. There exists other ways to form a first guess for the physical retrieval such as an average ozone profile from the ozonesonde training set. This is a focus of ongoing research.

5. Physical Retrieval

[22] The physical retrieval is based on the methodology of the AIRS science team algorithm [*Susskind et al.*, 2003] and compares an actual observed spectrum to one computed by the KCARTA forward model. The spectral range used in the physical retrieval is 970 cm^{-1} through 1084 cm^{-1}. Using a subset of the spectral range used in the statistical retrieval reduces computational time. Inputs to the physical retrieval include temperature and water vapor profiles, SAGE II stratospheric ozone climatology, ground ozone and the retrieved tropospheric ozone profile from the statistical retrieval. The algorithm then adjusts the tropospheric ozone in an iterative process to minimize the differences between the observed and calculated spectra.

[23] The physical retrieval begins with the simple assumption that the differences between the observed and calculated spectrum derive from the differences between the current ozone profile solution and the true ozone profile,

$$J^T \cdot U_J \Delta O' = \Delta R. \tag{12}$$

[24] The terms ΔR and J, refer to the observed minus calculated spectrum and the Jacobian matrix, respectively. The term $\Delta O'$ refers to the change to the current ozone profile solution in the rotated coordinate system in terms of the three layers; see below.

[25] The Jacobian matrix, J, quantifies the amount of spectral change caused by a specific change to the ozone profile,

$$J(i,j) = \frac{\partial r(j)}{\partial o(i)}. \tag{13}$$

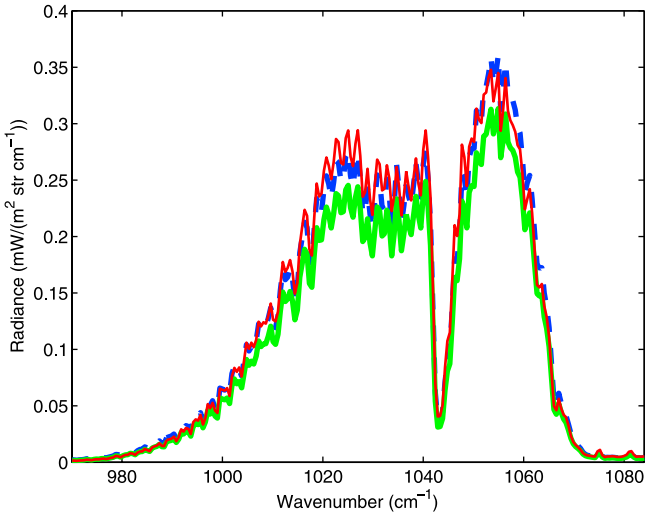

Figure 2. Spectral response to a 10% derivative to each of the three atmospheric layers in the physical retrieval. The dashed curve is for the layer from the ground up to 800 mbar. The thick solid curve is for the layer from 800 mbar to 600 mbar. The thin solid curve is for the layer from 600 mbar to 100 mbar.

In the equation above, $J(i, j)$ is the Jacobian at spectral channel, j, and layer, i, where j ranges from 1 to 239 and i ranges from 1 to 3. The $r(j)$ is the calculated radiance at spectral channel j and $o(i)$ is the perturbation to the ozone profile in layer i.The J matrix is constructed with forward model spectral calculations using KCARTA. The Jacobian matrix sections the troposphere into three distinct layers, surface to 800 mbar, 800 mbar to 600 mbar and 600 mbar to 100 mbar. Although these three layers cannot be distinguished with BBAERI spectra, the layers are retained to give the retrieval the freedom to determine the number of pieces of information in the spectra and where in the ozone profile the information resides. Figure 2 illustrates the Jacobian matrix, J, for a single iteration of the physical retrieval. Figure 2 shows the spectral change to be nearly identical for a 10% perturbation to each of the three layers. It is for this reason that there is only one piece of vertical information in the tropospheric ozone profile. Further illustration of this point can be seen in Figure 3 where the shape of the first-guess ozone profile is unchanged after the physical retrieval is complete.

[26] U_J is a unitary transformation matrix, whose dimensions are 3 by 3, consisting of the eigenvectors of the covariance of the Jacobian matrix. Like the statistical retrieval, the physical retrieval also is performed in a rotated coordinate system to constrain the solution. Solving equation (12) for $\Delta O'$ results in

$$\Delta O' = \left[U_J^T \cdot J \cdot W \cdot J^T \cdot U_J + H_J\right]^{-1} \cdot U_J^T \cdot J \cdot W \cdot \Delta R \quad (14)$$

$$W = W_q + W_T + W_n. \quad (15)$$

[27] The matrices H_J and W are the eigenvector weighting matrix and spectral noise compensation matrix, respectively. The H_J matrix weighs the eigenvectors much like the H matrix in equation (8). The W matrix is diagonally constructed using knowledge of the BBAERI instrument noise and the spectral contributions due to errors in the temperature and water vapor profiles used in the KCARTA calculations. The three matrices W_q, W_T and W_n refer to the spectral contributions from errors in the water vapor profile, errors in the temperature profile and instrument noise, respectively. The errors in the water vapor and temperature profiles stem from the fact that they too are retrieved quantities. The water vapor and temperature profiles are generated using the University of Wisconsin-Madison's retrieval code. The water vapor and temperature error statistics are used to calculate the spectral contributions, W_q and W_T, from each profile. The actual error statistics, ±5% in water vapor column and ±1 K at each level in the temperature profile, can be found in the literature [*Feltz et al.*, 2003].

[28] Equation (16) represents the amount of ozone profile change in the nonrotated coordinate system. This is the change in ozone profile ultimately applied to the current ozone profile solution.

$$\Delta O = U_J \cdot \Delta O'. \quad (16)$$

[29] After each iteration of the physical retrieval, the Jacobian matrix is recomputed and the process is repeated until the difference between the computed and observed spectrum is minimized. Errors for both the statistical and physical retrievals can be found in Table 2 and will be discussed in section 6.

6. Retrieval Validation

[30] During ABOVE03, 20 ozonesondes were flown primarily for AIRS validation. Using coincident lidar and

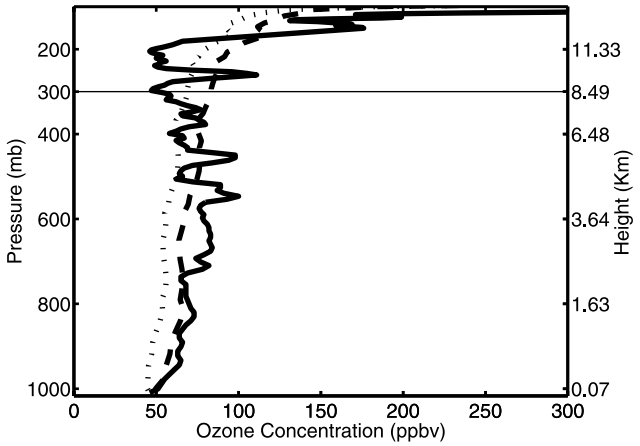

Figure 3. Retrieved ozone profile from 9 June 2003 at 1800 UTC. The thick solid, dotted, and dashed lines represent the ozone profile measured by the ozonesonde, the first guess from the statistical retrieval, and the final solution from the physical retrieval, respectively. The thin black line denotes the 300 mbar height. When integrated from the surface to 300 mbar, the first guess and the final solution showed errors of −33.4% and −1.8%, respectively, relative to the ozonesonde profile. The fine-scale features in the KLOBBER profile are an artifact of the statistical retrieval and should not be interpreted as profile information.

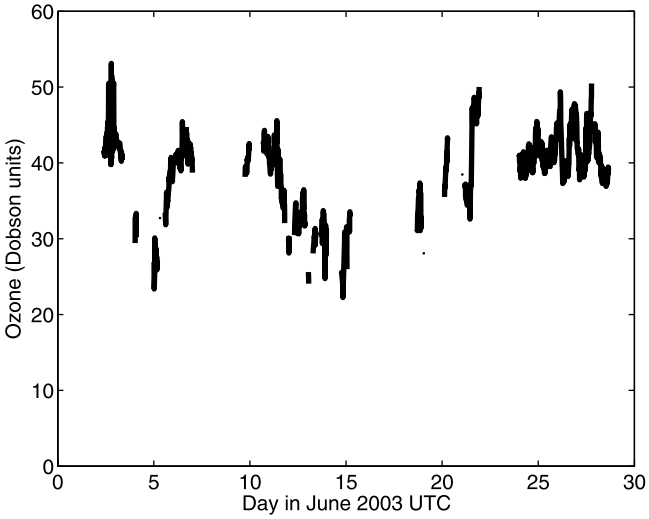

Figure 4. Retrieved tropospheric ozone column, surface to 300 mbar, for June 2003. Lack of data or cloud-contaminated BBAERI spectra cause the gaps in the time series.

all-sky images, 5 of the 20 ozonesonde flights were determined to be under exceptionally clear conditions. Using these 5 cases for validation of integrated column ozone from the surface up to 300 mbar, KLOBBER shows a mean bias of 1.6%, a root-mean-square (RMS) of 3.8% and a STandard Deviation (STD) of 4.2%; see Table 2. When applied to the background tropospheric ozone column of 42.6 DU for 2 June at Chesapeake Light, surface to 300 mbar, these results equate to a mean bias of 0.7 DU with an RMS of 1.7 DU and an STD of 1.8 DU. The background column ozone at Chesapeake Light will be discussed in more detail in section 7.

[31] Figure 3 illustrates an example of a full retrieval. The fine-scale features in the KLOBBER solution profile are an artifact of the statistical retrieval and should not be interpreted as profile information. Although KLOBBER is not capable of producing accurate ozone profiles, it has the ability to determine tropospheric column ozone from the surface up to 300 mbar with accuracy comparable to an ozonesonde whose errors range from ±3% to ±12% in the troposphere [*Newchurch et al.*, 2003; *Komhyr et al.*, 1995]. These error statistics translate to ±1.3 DU to ±5.1 DU when applied to the background column ozone, surface to 300 mbar on 2 June at Chesapeake Light. The advantage of KLOBBER is its ability to produce column ozone retrievals as long as the BBAERI instrument is functioning properly. Assuming clear skies, BBAERI produces a calibrated zenith-viewing spectrum every 8 to 10 min.

7. BBAERI Column Ozone Time Series

[32] The KLOBBER time series of integrated column ozone, surface to 300 mbar, was produced from BBAERI measurements acquired at the United States Coast Guard Chesapeake Light lighthouse platform (36.91°N, 75.71°W, 14 miles due east of Virginia Beach, Virginia), during ABOVE03 conducted from 28 May to 9 July 2003; see Figure 4 [*Lightner*, 2004]. Other instruments present at Chesapeake Light during ABOVE03 were ozonesondes, a Sun photometer, an elastic lidar system and surface ozone UV photometers. The ozonesondes flown during ABOVE03 utilized electrochemical cell ozone detectors and flew along with standard Vaisala RS-80s radiosondes. The AErosol RObotic NETwork (AERONET) Sun photometer present during ABOVE03 measures aerosol optical depths and total column water vapor (B. Holben, personal communication, 2008). The Elastic Lidar Facility (ELF) was run side by side with BBAERI during AIRS overpasses at Chesapeake Light during ABOVE03 [*McCann et al.*, 2003; *McMillan et al.*, 2003]. Also, two in situ ozone instruments were deployed to provide a continuous record of surface ozone. One was a TEI Model 49c photometer set up inside the lighthouse with a teflon inlet line to the outside, and the other was a UV instrument packaged for use at sea mounted under the main deck of the lighthouse [*Hintsa et al.*, 2004]. The measurements recorded by these instruments will be discussed later in this paper.

[33] The first indication of an ozone anomaly is the magnitude of the tropospheric ozone column measured using the KLOBBER algorithm. 2 June 2003 displayed tropospheric ozone column amounts as high a 53.1 DU; see Figure 5. The remainder of the ABOVE03 time series was well below this amount with an average of 39.7 DU and an STD of 4.7 DU. While this average is high compared to the 1624 northern hemispheric ozonesondes from the statistical retrieval training set whose average tropospheric column is 27.5 DU with an STD of 7.6 DU, it is not unexpected. Previous measurements show elevated tropospheric ozone down-wind of urban areas of the United States as a result of pollution emissions [*Fast et al.*, 2002; *Ryan et al.*, 1998]. Ozone enhancements off the east coast of the United States have been measured as far down-wind as Bermuda [*Moody et al.*, 1995].

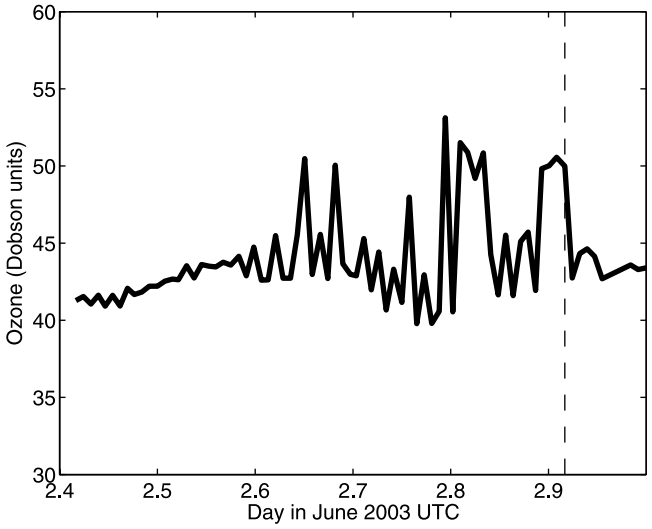

Figure 5. KLOBBER tropospheric ozone time series retrieved from BBAERI radiances on 2 June 2003 at Chesapeake Light. Integrated tropospheric column from the surface to 300 mbar. The solid and dashed lines represent the KLOBBER time series and the ozonesonde flight time respectively. The retrieved tropospheric column at the time of the ozonesonde flight was 49.9 DU.

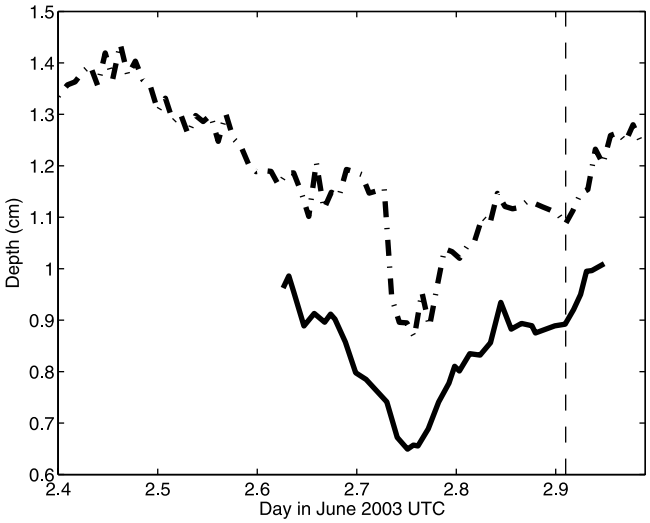

Figure 6. Column water vapor from 2 June 2003. The solid, dotted, and dashed lines represent the AERONET time series, BBAERI time series, and the ozonesonde flight time, respectively. Both the AERONET and BBAERI data observe a significant decrease in column water vapor midafternoon local time (UTC minus 4 h). Note that this is level 2.0 AERONET data.

[34] The large spectrum-to-spectrum variations in column ozone, beginning around decimal day June 2.6 (1424 UTC), present the second indication of an ozone anomaly. The largest of these spikes, about 13 DU, occurred around decimal day 2.8 (1912 UTC) and was well above the estimated error of the KLOBBER algorithm. The variations in tropospheric column ozone likely result from filaments of enhanced ozone in an overlying smoke plume and a stratospheric intrusion as discussed in more detail in sections 8 and 10.

[35] Temperature and water vapor profiles also are retrieved from BBAERI spectra with the use of the University of Wisconsin-Madison's retrieval code. The integrated water column, surface to 300 mbar, displays a minimum of 0.87 cm during 2 June; see Figure 6. This is the lowest amount observed during ABOVE03, whose maximum water column was 5.2 cm with an average of 3.0 cm and an STD of 1.2 cm. This extremely low water column on 2 June is confirmed by both an ozonesonde and the AERONET instrument measurements from Chesapeake Light and could indicate stratospheric air. The AERONET data will be discussed in more detail in section 9.

8. Ozonesonde

[36] The ozonesonde flown at decimal day June 2.91 (2156 UTC) displayed a thick layer of enhanced ozone between 750 and 450 mbar; see Figure 7. As noted in Figure 5, the ozonesonde flight time was coincident with one of the column ozone spikes retrieved from BBAERI spectra. At the time of launch, the KLOBBER algorithm retrieved a tropospheric ozone column from the surface to 300 mbar of 49.9 DU. The ozonesonde measured 46.1 DU. The pressure-weighted average ozone mixing ratio in the enhanced layer was 94.9 parts per billion by volume (ppbv) with a layer integrated column of 22.6 DU. This is in contrast to the region below the enhanced layer 1017 to 750 mbar, whose pressure-weighted average ozone mixing ratio was 61.8 ppbv with a layer integrated column of 14.4 DU. The region above the enhanced layer 450 to 300 mbar, had a pressure-weighted average ozone mixing ratio of 76.9 ppbv and a layer integrated column of 9.1 DU.

[37] Calculations were conducted to see if the enhanced layer seen by the ozonesonde can account for the increase in the tropospheric column detected by KLOBBER. The enhanced layer was removed by linearly interpolating the ozone mixing ratio between 750 mbar and 450 mbar using the pressure-weighted average ozone mixing ratios above and below the enhanced layer as endpoints; see Figure 7. The points used to bound the interpolation below and above the enhanced layer, used the pressure-weighted averages from 900 to 750 mbar and 450 to 300 mbar, respectively. The integrated tropospheric column ozone excluding the enhanced layer results in a value of 41.0 DU, close to the background for this period of the time series, 42.6 ± 0.9 DU. This background was estimated from the average tropospheric ozone column from the surface to 300 mbar for 4 h before and after the anomalous spikes. In decimal time of day this would be day June 2.42 to 2.59 (1005 to 1409 UTC) and 2.97 to 3.20 (2316 to 0448 UTC). This same calculation performed during the period of the anomalous spikes, decimal day June 2.59 to 2.97 (1409 to 2316 UTC), resulted in an average of 44.9 DU with an STD of 3.6 DU.

[38] As illustrated in Figure 8, the ozonesondes' relative humidity profile exhibits a dramatic decrease near 850 mbar (boundary layer top) and a steady decrease up to approximately 450 mbar. The particularly dry layer from about 550 mbar to 475 mbar coincides with the uppermost, and highest mixing ratio O_3 layer with a peak value of 123 ppbv. The average relative humidity from 850 mbar to 450 mbar was 6.3% with a minimum of 2.0% between 550 mbar and

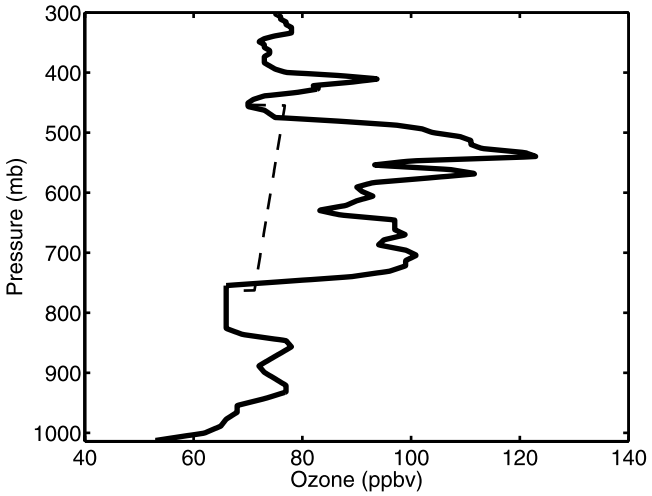

Figure 7. Ozonesonde flown on 2 June 2003 at 2156 UTC. The solid and dashed lines represent the ozone profile and the ozone profile minus the enhanced layer, respectively. Excluding the enhanced layer causes the tropospheric ozone column to return to its background amount. The enhanced layer has an average ozone mixing ratio of 94.9 ppbv.

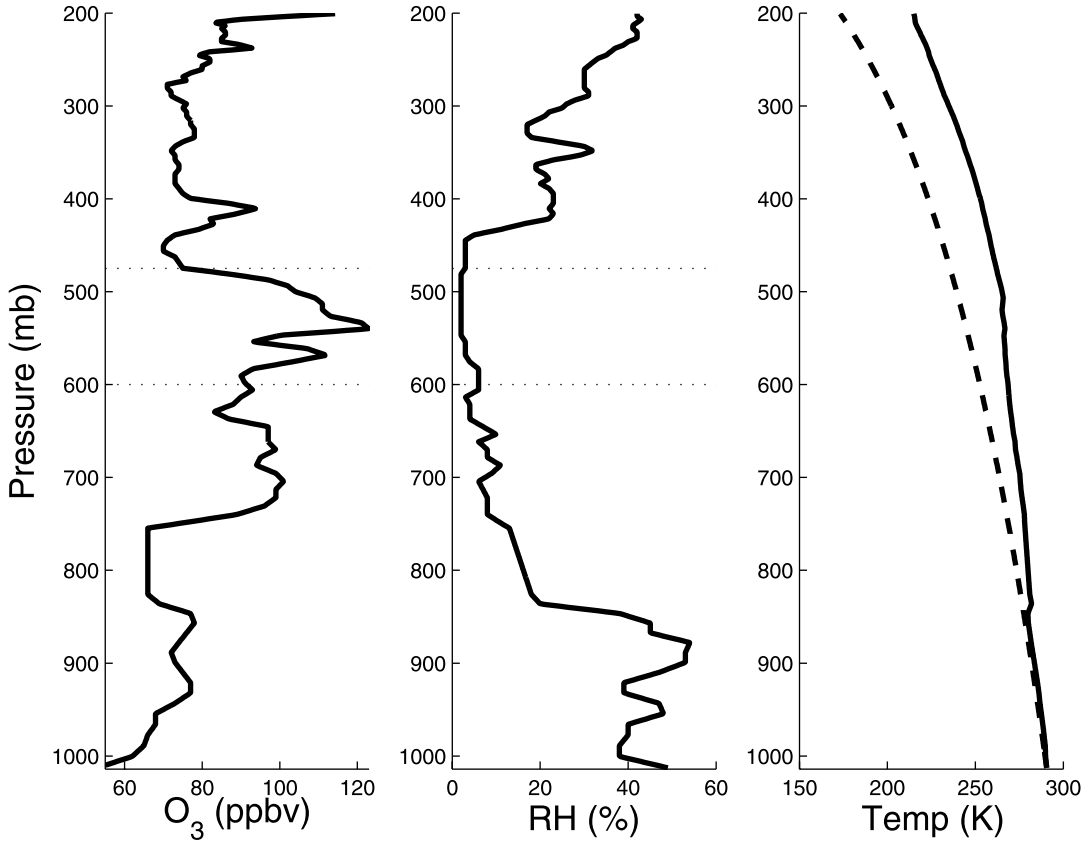

Figure 8. Ozonesonde from 2 June 2003 at 2156 UTC. The humidity profile exhibits a significant dropoff of water in the midtroposphere. The area between the dotted lines shows the maximum amount of ozone within the enhanced layer coincident with the minimum in humidity. Above and just below the enhanced layer (750 mbar to 450 mbar), the temperature profile roughly follows a dry adiabatic lapse rate. The temperature profile (solid line) displays a notable deviation from a dry adiabatic lapse rate (dashed line) within the enhanced layer.

475 mbar. The average relative humidity from 850 mbar to 450 mbar for the 1624 northern hemispheric ozonesondes in the statistical retrieval training set is 39.2% with an average minimum value of 15.4%. This coincident drop in relative humidity and dramatic increase in ozone suggests that some of the air in this layer originated in the stratosphere.

[39] The region from 850 mbar to 550 mbar does exhibit enhanced ozone and very low relative humidity but the lidar measurements and satellite images show that there may be more than just stratospheric air causing the anomaly. The satellite images show smoke from biomass burning moving into the region from Canada on 2 June. The presence of the smoke plume also can be seen in the lidar time series. Both will be discussed later.

[40] The temperature profile exhibits several features of interest. Below about 850 mbar the temperature roughly follows a dry adiabatic lapse rate, indicative of a well-mixed boundary layer. Between 850 mbar and 450 mbar the lapse rate becomes subadiabatic. With such a low relative humidity throughout this deep layer, the decrease in the lapse rate could not have been caused by condensation. The additional heating in this layer could come from solar heating of a thick aerosol layer, possibly smoke, and perhaps adiabatic heating of subsiding stratospheric air. Above 450 mbar the temperature profile returns to a dry adiabatic lapse rate. Although the ozonesonde alone is unable to determine whether the heating in the 850 to 450 mbar layer was caused by solar heating and/or subsidence heating, it definitively shows anomalous tropospheric layers.

9. AERONET

[41] On 2 June 2003, the AERONET instrument detected an anomaly in the total column water vapor; see Figure 6. The backscatter time series from the ELF lidar system present at Chesapeake Light during ABOVE03, shows the aerosol layer thinning significantly around the time of the AERONET column water vapor anomaly. Although there are no level 2.0 AERONET aerosol optical depth measurements during the period of time when the aerosol layer was thinning, the AERONET optical depths tracked very well with the ELF 532 nm aerosol optical depths; see Figure 9. The ELF measurements will be discussed in more detail in section 10.

[42] The total column water vapor exhibits a significant decrease starting around decimal day June 2.65 (1536 UTC) and reaching its minimum value at June 2.75 (1800 UTC); see Figure 6. The total column water vapor retrieved from BBAERI shows a similar decrease, but with a much sharper onset at decimal day June 2.73 (1731 UTC). The differences

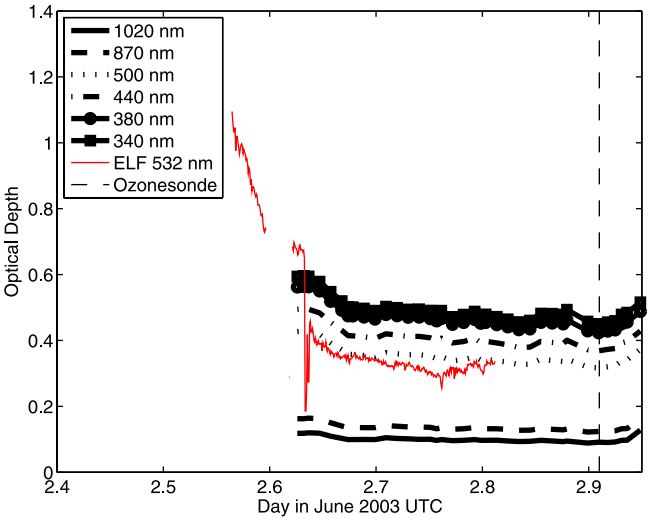

Figure 9. AERONET and ELF aerosol optical depth from 2 June 2003. Aerosol optical depth shows a drastic decrease late in the day. The ELF lidar 532 nm aerosol optical depth tracks well with the AERONET observations. Note that this is level 2.0 AERONET data.

between AERONET and BBAERI total water vapor columns could result from differences in the orientation of the instruments' fields-of-view. Because AERONET uses the sun as a radiation source, the instrument would have been pointing slightly south of the lighthouse. BBAERI, however, looks straight up at the zenith to acquire the spectra used to retrieve temperature, water vapor and other trace gases.

10. Lidar

[43] During 2 June 2003, the ELF lidar detected a significant aerosol layer nearly 1 km thick starting at about 800 mbar; see Figures 10 and 11. The aerosol layer persisted for the majority of the day and then dissipated by day's end. Unfortunately there is no lidar data during the actual time of the ozonesonde flight. An ozonesonde was launched for the AIRS PM overpass during the PM lidar time series but failed owing to technical problems. A second ozonesonde was launched after the technical problems were solved, but this was not until nearly 2 h after the lidar shutdown. However, the portion of the lidar time series closest in time to the ozonesonde launch does supply additional insight to the ozonesonde profiles.

[44] The air above 550 mbar in the lidar time series exhibits a relative lack of aerosols. This supports the argument that the air is of stratospheric origin as suggested by the ozonesonde profiles. The thick aerosol layer seen in the lidar time series from about 850 mbar to 550 mbar closest in time to the ozonesonde launch gives further evidence for the presence of a smoke layer. Coincident elevated amounts of ozone and aerosols could be the result of photochemical oxidation of biomass burning products in the smoke plume over the region during this period of time. It has been shown that significant amounts of ozone can result from photochemical aging of forest fire smoke plumes [*Lapina et al.*, 2006].

[45] The ELF 532 nm aerosol optical thickness PM time series agrees well with the AERONET optical thicknesses from the same period of time; see Figure 9. However, the ELF aerosol optical depth shows no correlation with either the KLOBBER tropospheric ozone column time series or the total column water vapor time series. One possible explanation for this is the smoke layer and the stratospheric air above it could have mixed in such a way that the aerosol optical thickness remained constant while the tropospheric ozone column and total column water vapor varied significantly. Or, perhaps more likely, the smoke and stratospheric intrusion occur in distinct layers with different variability.

11. Satellites

[46] The MOderate resolution Imaging Spectrometer (MODIS) on board the NASA Terra satellite and the Total

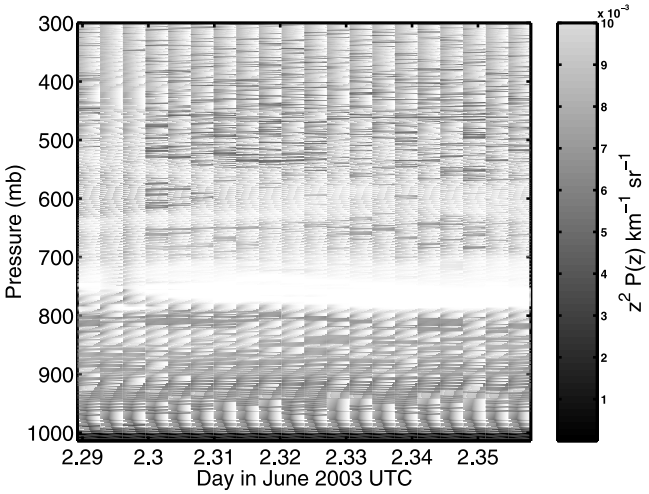

Figure 10. The ELF lidar backscatter time series exhibits an optically thick layer at about 2.5 km (800 mbar) which lasted for the majority of the day. This shows the lidar time series for the AIRS AM overpass.

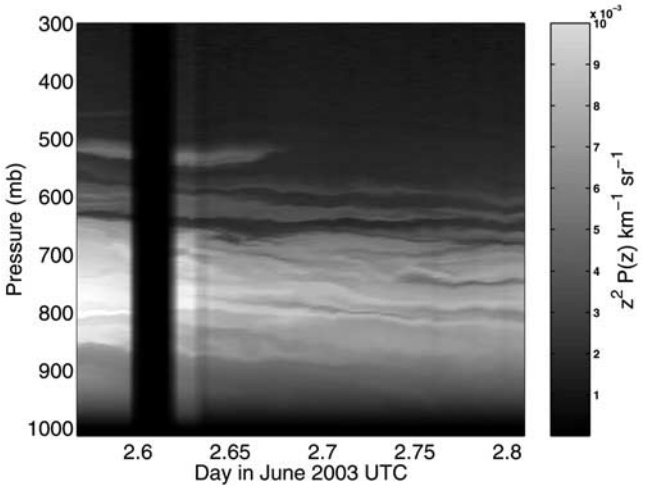

Figure 11. The ELF lidar backscatter time series for the AIRS PM overpass shows the aerosol layer starts to thin by day's end.

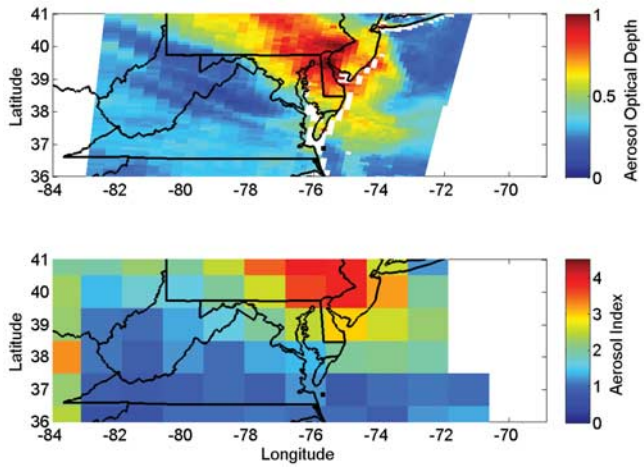

Figure 12. (top) Terra MODIS level 2 aerosol optical depth measured 2 June 2003 at 1532 UTC and (bottom) TOMS Version 8 aerosol index on 2 June 2003 clearly show a thick plume covering the Delmarva peninsula. The very edge of the plume is over the area of the lighthouse, which may explain the spikes in the KLOBBER time series. The location of Chesapeake is indicated by the black square. The white areas represent lack of data.

Ozone Mapping Spectrometer (TOMS) on board the NASA Earth Probe satellite, measured the progress of a smoke plume toward the eastern United States from eastern Russia on the days leading up to 2 June 2003 [*Damoah et al.*, 2004]. The aerosol optical depth products on 2 June clearly show the Siberian smoke plume moving down from Canada over the area of the lighthouse; see Figure 12. The optical depth of the smoke plume measured by MODIS over central and southeastern Maryland is almost triple that of the surrounding areas of central Virginia and New Jersey. The TOMS instrument confirms the MODIS measurements showing the aerosol index of the plume to be about three times that of the surrounding areas. The leading edge of this smoke plume in the vicinity of Chesapeake Light suggests photochemical ozone production in biomass burning material as a contributor to the observed tropospheric ozone anomaly. The lidar data place this smoke plume between 850 and 550 mbar.

[47] Ozone and carbon monoxide often show positive correlation in the presence of pollution and intense solar radiation [*Kajii et al.*, 1998; *Chameides and Walker*, 1973]. The 500 mbar carbon monoxide measurements made by AIRS onboard the NASA Aqua satellite substantiate the hypothesis that the elevated aerosol measurements made by MODIS and TOMS are due to a smoke plume; see Figure 13 [*McMillan et al.*, 2008, 2005]. Carbon monoxide acts as a good indicator of smoke from fossil fuel and biomass burning because large amounts of the compound are released by combustion of these materials. The measurements from AIRS, MODIS and TOMS all indicate that the edge of the smoke plume passed over Chesapeake Light on 2 June. At the edge of a smoke plume, it is expected that the aerosol and pollution content would vary significantly. This may explain the large spikes seen in the KLOBBER ozone time series.

12. Potential Vorticity

[48] Using data from the National Center for Environmental Prediction (NCEP) Aviation model (AVN), maps of potential vorticity (PV) at 250 mbar were generated for 2 June 2003; see Figure 14. The maps show large values of PV over the northeastern and mid-Atlantic United States, suggesting the presence of stratospheric air in the upper troposphere. Thus, we deduce that stratospheric air accounts for the drop in tropospheric water vapor measured by BBAERI and AERONET and caused the dry layer of enhanced ozone encountered by the ozonesonde. A stratospheric intrusion could also be responsible, in part, for the enhanced ozone levels measured by the KLOBBER ozone retrieval. Furthermore, we propose that intermittent filaments of this stratospheric intrusion are responsible for the variations in total column ozone retrieved by KLOBBER on 2 June. Although the PV maps lack the horizontal

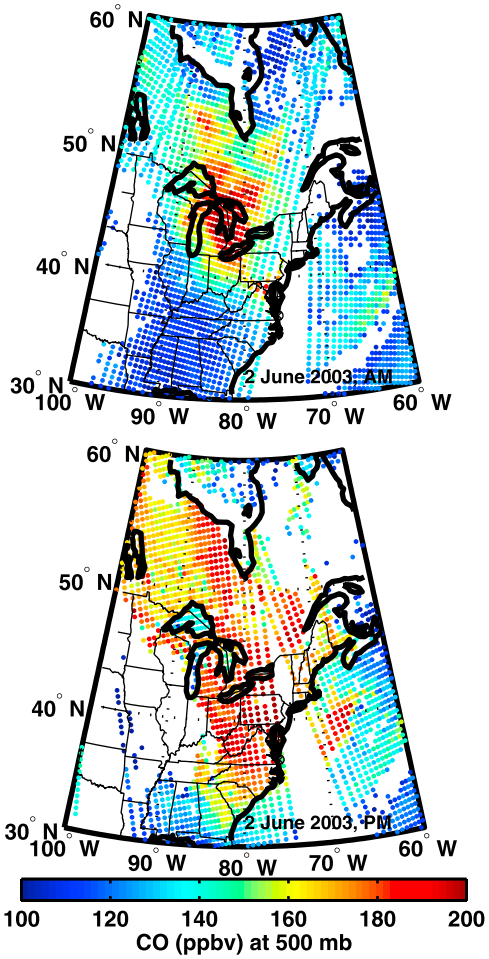

Figure 13. AIRS 500 mbar carbon monoxide measurements for both the (top) AM and (bottom) PM overpasses on 2 June 2003. Increased levels of carbon monoxide are clearly visible over the Delmarva peninsula and are spatially and temporally coincident with the aerosol plume observed by MODIS and TOMS.

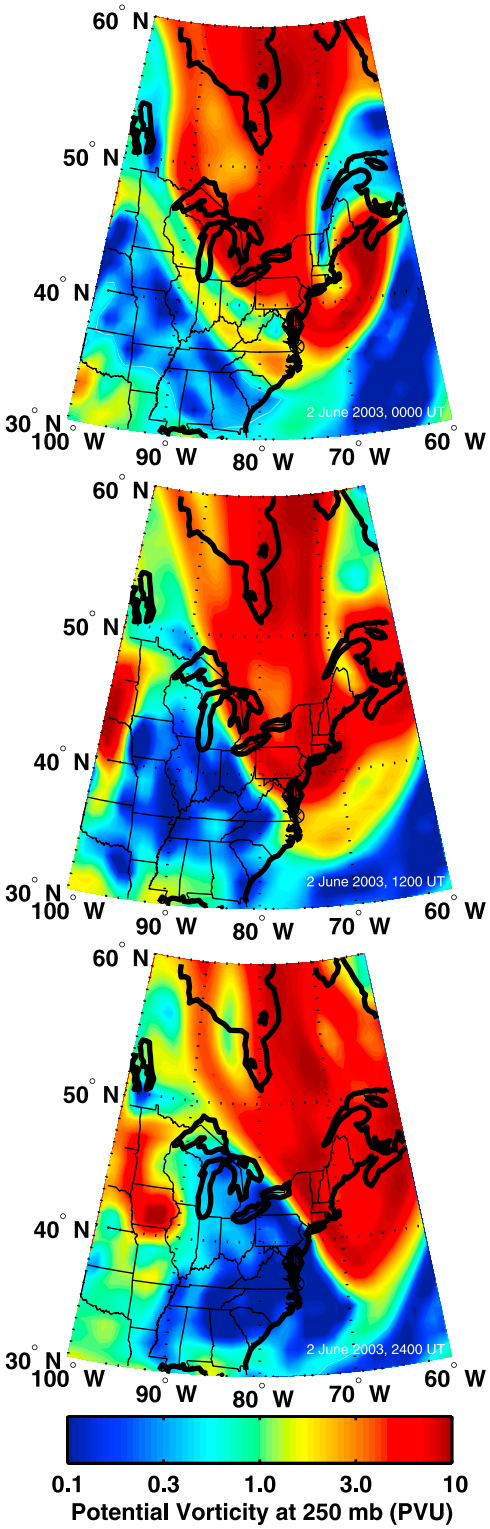

Figure 14. Maps of 250 mbar potential vorticity derived from NCEP AVN model. The maps give strong indication of tropopause folding in the area of Chesapeake Light on 2 June 2003 at (top) 0000 UTC, (middle) 1200 UTC, and (bottom) 2400 UTC.

resolution to observe such fine-scale structure, they do reveal stretching and pinching off along the mid-Atlantic coast on 2 June.

13. Conclusions

[49] The KLOBBER algorithm exhibits a mean bias in tropospheric column O_3 of 1.6%, an RMS of 3.8% and an STD of 4.2% when compared to in situ ozonesondes flown during ABOVE03. When applied to the background tropospheric ozone column of 42.6 DU for 2 June at Chesapeake Light, surface to 300 mbar, these results equate to a mean bias of 0.7 DU with an RMS of 1.7 DU and an STD of 1.8 DU. These retrieval errors are small in comparison to the spikes observed in the tropospheric column ozone time series on this day which were on the order of 10 DU. A coincident ozonesonde O_3 profile shows several layers of enhanced O_3 between 450 and 850 mbar.

[50] The ozonesonde water vapor profile and total column water vapor from both AERONET and BBAERI strongly suggest at least some of the observed enhanced tropospheric ozone originated in the stratosphere. Computations of potential vorticity using data from the NCEP AVN model suggest that tropopause folding may have contributed to the enhanced tropospheric ozone column detected by the KLOBBER ozone retrieval. Lidar data from Chesapeake Light along with MODIS, TOMS and AIRS data point to the possibility that some of the enhanced tropospheric ozone could have resulted from photochemical oxidation within a smoke plume.

[51] These results illustrate the ability of BBAERI and the KLOBBER algorithm to produce an integrated tropospheric ozone time series sensitive enough to detect tropospheric ozone anomalies. Although KLOBBER cannot distinguish between photochemically produced ozone and ozone intruding from the stratosphere, when combined with other remote sensing observations such as lidar and satellites, tropospheric ozone origins can be deduced. Moreover, the temporal resolution afforded by BBAERI or another AERI-like instrument enables more detailed investigation of these types of events and pollution monitoring

[52] **Acknowledgment.** Special thanks go to Brent Holben for supplying AERONET data from the COVE site and to Ken Rutledge for making the use of Chesapeake Light a possibility. We would also like to thank Michele McCourt, Eric Maddy, Ray Rogers, Felicita Russo, and Jing Song for their hard work and long hours during ABOVE03. We would like to thank Lynn Sparling for supplying us with the potential vorticity figures. Finally, we gratefully thank NASA for its support through grant NAG5-1156-7 for AIRS Validation and grant NNG04GN42G for development of AIRS trace gas products, and through a subcontract with JPL on the AIRS Project prime contract NAS7-03001 for continuing optimization and validation of AIRS trace gas products.

References

Chameides, W., and J. Walker (1973), A photochemical theory of tropospheric ozone, *J. Geophys. Res.*, *78*(36), 8751–8760.

Damoah, R., N. Spichtinger, C. Forster, P. James, I. Mattis, U. Wandinger, S. Beirle, T. Wagner, and A. Stohl (2004), Around the world in 17 days-hemispheric-scale transport of forest fire smoke from Russia in May 2003, *Atmos. Chem. Phys.*, *4*, 1311–1321.

De Backer-Barilly, M. R., and D. Courtois (1997), Intensity measurments of ozone lines in the ν_3 band, *Appl. Phys. B*, *64*, 607–611.

Devi, V. M., D. C. Benner, M. A. H. Smith, and C. P. Rinsland (1997), Air-broadening and shift coefficients of O_3 lines in the ν_2 band and their temperature dependence, *J. Mol. Spectrosc.*, *182*, 221–238.

Engelen, R. J., and G. L. Stephens (1997), Infrared radiative transfer in the 9.6-μm band: Application to TIROS operational vertical sounder ozone retrieval, *J. Geophys. Res.*, *102*(D6), 6929–6939.

Fast, J. D., R. A. Zaveri, X. Bian, E. G. Chapman, and R. C. Easter (2002), Effect of regional-scale transport on oxidants in the vicinity of Philadelphia during the 1999 NE-OPS field campaign, *J. Geophys. Res.*, *107*(D16), 4307, doi:10.1029/2001JD000980.

Feltz, W. F., W. L. Smith, R. O. Knuteson, H. E. Revercomb, H. M. Woolf, and H. B. Howell (1998), Meteorological applications of temperature and water vapor retrievals from the ground-based Atmospheric Emitted Radiance Interferometer (AERI), *J. Appl. Meteorol.*, *37*, 857–875.

Feltz, W. F., W. L. Smith, H. B. Howell, R. O. Knuteson, H. M. Woolf, and H. E. Revercomb (2003), Near-continuous profiling of temperature, moisture, and atmospheric stability using the Atmospheric Emitted Radiance Interferometer (AERI), *J. Appl. Meteorol.*, *42*, 584–597.

Flaud, J. M., C. Camy-Peyret, V. M. Devi, C. P. Rinsland, and M. A. H. Smith (1987), The ν_1 and ν_3 bands of $^{16}O_3$: Line positions and intensities, *J. Mol. Spectrosc.*, *124*, 209–217.

Gong, H., P. W. Bradly, M. S. Simmons, and D. P. Tashkin (1986), Impaired exercise performance and pulmonary function in elite cyclists during low-level ozone exposure in a hot environment, *Am. Rev. Respir. Dis.*, *134*, 726–733.

Herzberg, G. (1971), *The Spectra and Structures of Simple Free Radicals: An Introduction to Molecular Spectroscopy*, Cornell Univ. Press, Ithaca, N. Y.

Hintsa, E., et al. (2004), A new ozone measurement system for autonomous measurments from ocean buoys and towers, *J. Atmos. Oceanic Technol.*, *21*, 1007–1016.

Kajii, Y., K. Someno, H. Tanimoto, J. Hirokawa, H. Akimoto, T. Katsuno, and J. Kawara (1998), Evidence for the seasonal variation of photochemical activity of tropospheric ozone: Continuous observation of ozone and CO at Happo, Japan, *Geophys. Res. Lett.*, *25*(18), 3505–3508.

Kehrl, H. R., D. B. Penden, B. Ball, L. J. Folinsbee, and D. Horstman (1999), Increased specific airway reactivity of persons with mild allergic asthma after 7.6 hours of exposure to 0.16 ppm ozone, *J. Allergy Clin. Immunol.*, *104*(6), 1198–1204.

Komhyr, W., R. Barnes, G. Brothers, J. Lathrop, and D. Opperman (1995), Electrochemical concentration cell ozonesonde performance evaluation during STOIC 1989, *J. Geophys. Res.*, *100*(D5), 9231–9244.

Lapina, K., R. Honrath, M. Owen, V. Martin, and G. Pfister (2006), Evidence of significant large-scale impacts of boreal fires on ozone levels in the midlatitude Northern Hemisphere free troposphere, *Geophys. Res. Lett.*, *33*, L10815, doi:10.1029/2006GL025878.

Lefohn, A., S. Oltmans, T. Dann, and H. Singh (2001), Present-day variability of background ozone in the lower troposphere, *J. Geophys. Res.*, *106*(D9), 9945–9958.

Lightner, K. J. (2004), A tropospheric ozone retrieval using a ground-based up-looking infrared interferometer, Ph.D. thesis, Univ. of Md. Baltimore County, Baltimore.

Luo, M., R. Beer, D. J. Jacob, J. A. Logan, and C. D. Rodgers (2002), Simulated observation of tropospheric ozone and CO with the Tropospheric Emission Spectrometer (TES) satellite instrument, *J. Geophys. Res.*, *107*(D15), 4270, doi:10.1029/2001JD000804.

Marenco, A. (1986), Variations of CO and O_3 in the troposphere: Evidence of O_3 photochemistry, *Atmos. Environ.*, *20*(5), 911–918.

McCann, K. J., R. M. Hoff, R. Rogers, J. Comer, W. McMillan, C. Barnet, J. Gou, S. DeSouza-Machado, and L. Strow (2003), A comparison of measurements of cloud optical depth made from the AIRS/AQUA instrument and the UMBC Elastic Lidar Facility (ELF), paper presented at International Symposium on Tropospheric Profiling: Needs and Technologies, Liebniz Inst. for Tropos. Res., Leipzig, Germany.

McConnell, R., K. Berhane, F. Gilliland, S. London, T. Islam, W. Gauderman, E. Avol, H. Margolis, and J. Peters (2002), Asthma in exercising children exposed to ozone: A cohort study, *Lancet*, *359*, 386–391.

McDonnell, W. F., H. W. Kehrl, S. Abdul-Salaam, P. J. Ives, L. J. Folinsbee, and R. B. Devlin (1991), Respiratory responce of humans exposed to low levels of ozone for 6.6 hours, *Arch. Environ. Health*, *46*(3), 145–150.

McMillan, W. W., et al. (2003), ABOVE03, the 2003 AIRS BBAERI Ocean Validation Experiment: AIRS validation and aerosols, *EOS Trans. AGU*, *84*(46), Abstract H32B-0572.

McMillan, W. W., C. Barnet, L. Strow, M. Chahine, M. McCourt, P. Novelli, S. Korontzi, E. Maddy, and S. Datta (2005), Daily global maps of carbon monoxide: First views from NASA's Atmospheric Infrared Sounder, *Geophys. Res. Lett.*, *32*, L11801, doi:10.1029/2004GL021821.

McMillan, W. W., et al. (2008), AIRS views of transport from 12 to 22 July 2004 Alaskan/Canadian fires: Correlation of AIRS CO and MODIS AOD with forward trajectories and comparison of AIRS CO retrievals with DC-8 in-situ measurements during INTEX-A/ICARTT, *J. Geophys. Res.*, *113*, D20301, doi:10.1029/2007JD009711.

Moody, J. L., S. J. Oltmans, H. Levy II, and J. T. Merrill (1995), Transport climatology of tropospheric ozone: Bermuda, 1988–1991, *J. Geophys. Res.*, *100*(D4), 7179–7194.

Nalli, N. R., P. J. Minnett, E. Maddy, W. W. McMillan, and M. D. Goldberg (2008), Emissivity and reflection model for calculating unpolarized isotropic water surface-leaving radiance in the infrared. 2: Validation using Fourier transform spectrometers, *Appl. Opt.*, *47*(25), 4649–4671.

Newchurch, M., M. Ayoub, S. Oltmans, B. Johnson, and F. Schmidlin (2003), Vertical distribution of ozone at four sites in the United States, *J. Geophys. Res.*, *108*(D1), 4031, doi:10.1029/2002JD002059.

Olsen, M., and J. L. Stanford (2001), Evidence of stratosphere-to-troposphere transport within a mesoscale model and Total Ozone Mapping Spectrometer total ozone, *J. Geophys. Res.*, *106*(D21), 27,323–27,334.

Parrish, D. D., J. S. Holloway, M. Trainer, P. Murphy, G. L. Forbes, and F. C. Fehsenfeld (1993), Export of North American ozone pollution to the North Atlantic Ocean, *Science*, *259*, 1436–1439.

Rothman, L. S., et al. (1998), The HITRAN molecular spectroscopic database and HAWKS (HITRAN Atmospheric Workstation) 1996 edition, *J. Quant. Spectrosc. Radiat. Transfer*, *60*, 665–710.

Ryan, W. F., B. G. Doddridge, R. R. Dickerson, R. M. Morales, K. A. Hallock, P. T. Roberts, D. L. Blumenthal, J. A. Anderson, and K. L. Civerolo (1998), Pollutand transport during a regional O_3 episode in the mid-Atlantic states, *J. Air Waste Manage. Assoc.*, *48*, 786–797.

Sinha, A., and R. Toumi (1997), Tropospheric ozone, lightning, and climate change, *J. Geophys. Res.*, *102*(D9), 10,667–10,672.

Smith, M. A. H., V. M. Devi, D. C. Benner, and C. P. Rinsland (1997), Temperature dependence of air-broadening and shift coefficients of O_3 lines in the ν_1 band, *J. Mol. Spectrosc.*, *182*, 239–259.

Smith, M. A. H., V. Malathy, D. C. Benner, and C. P. Rinsland (2001), Absolute intensities of $^{16}O_3$ lines in the 9–11 μm region, *J. Geophys. Res.*, *106*(D9), 9909–9921.

Strow, L., H. Motteler, R. Benson, S. Hannon, and S. De Souza-Machado (1998), Fast computation of monochromatic infrared atmospheric transmittances using compressed look-up tables, *J. Quant. Spectrosc. Radiat. Transfer*, *59*, 481–493.

Strow, L. L., S. E. Hannon, S. De Souza-Machado, H. Motteler, and D. Tobin (2003), Overview of the AIRS radiative transfer model, *IEEE Trans. Geosci. Remote Sens.*, *41*, 303–313.

Sudo, K., and M. Takahashi (2001), Simulation of tropospheric ozone changes during 1997–1998 El Niño: Meteorological impact on tropospheric photochemistry, *Geophys. Res. Lett.*, *28*(21), 4091–4094.

Susskind, J., C. D. Barnet, and J. M. Blaisdell (2003), Retrieval of atmospheric and surface parameters from AIRS/AMSU/HSB data in the presence of clouds, *IEEE Trans. Geosci. Remote Sens.*, *41*, 390–409.

Thompson, A. M. (1984), The effect of clouds on photolysis rates and ozone formation in the unpolluted troposphere, *J. Geophys. Res.*, *89*(D1), 1341–1349.

Thompson, A. M. (2003), Tropical tropospheric ozone: A perspective on photochemical and dynamical interactions from observations in the past five years, *IGAC Activities Newsl.*, *28*, 6–11.

Thompson, A., et al. (2003a), Southern Hemisphere additional ozonesondes (shadoz) 1998–2000 tropical ozone climatology: 1. Comparison with total ozone mapping spectrometer (TOMS) and ground-based measurements, *J. Geophys. Res.*, *108*(D2), 8238, doi:10.1029/2001JD000967.

Thompson, A., et al. (2003b), Southern Hemisphere additional ozonesondes (shadoz) 1998–2000 tropical ozone climatology: 2. Tropospheric variability and the zonal wave-one, *J. Geophys. Res.*, *108*(D2), 8241, doi:10.1029/2002JD002241.

Van Delst, P. (1996), Ozone concentration profile retrieval from ground-based high-resolution thermal infrared spectra, Ph.D. thesis, Curtin Univ. of Technol., Perth, West. Aust., Australia.

C. D. Barnet, STAR, NESDIS, NOAA, Camp Springs, MD 20746, USA.

E. J. Hintsa, Woods Hole Oceanographic Institution, Woods Hole, MA 02543, USA.

R. M. Hoff, K. J. McCann, and W. W. McMillan, Department of Physics, University of Maryland Baltimore County, Baltimore, MD 21250, USA.

K. J. Lightner, Applied Signal Technology, Inc., 306 Sentinel Drive, Suite 100, Annapolis Junction, MD 20701, USA. (kurt_lightner@appsig.com)

M. J. Newchurch, Department of Atmospheric Science, University of Alabama in Huntsville, Huntsville, AL 35899, USA.